Comparison of Aerodynamic Parameters and Power Conversion of a Four-flapping-wing Robot in Different Flight Modes

Kamonrat Tangudomkit and Pruittikorn Smithmaitrie*
Department of Mechanical and Mechatronics Engineering, Faculty of Engineering, Prince of Songkla University, Hat Yai, Songkhla, Thailand
*Email: pruittikorn.s@psu.ac.th

***Abstract*—In order to develop a flapping wing robot, the principles of flapping behavior must be understood. In this study, a robot with four flapping wings was investigated to determine the aerodynamic flight parameters and power conversion under three conditions. These are 1) the flapping test on a fixed base to investigate the relationship between the electrical power, the velocity profile of the air jet behind the wings, and the thrust, 2) the hovering test to determine the power requirement that generates the hovering thrust, and 3) the vertical flight test to investigate the power conversion between the input electrical power and the output aerodynamic power. The result of the air velocity profile shows that the maximum jet velocity occurred at 22.5 degrees relative to the body orientation. The flapping wing robot hovered with an average thrust of 0.118 N, with the thrust oscillated around the body weight of 0.123 N. The hovering aerodynamic power-to-weight ratio was 0.020 W/g. The experiments on the different flight modes show the specific conversion of electric power to aerodynamic power of the four-wing robot, which could be used as a guiding parameter for the design of the actuator, flapping mechanism, or wing geometry for further development of four-wing robots.**

***Index Terms*—Flapping wing robot, aerodynamic parameters, hovering flight, flight test, thrust, power conversion**

I. Introduction

Flapping wing micro aerial vehicles (FWMAVs) have long been a fascinating topic for inventors and researchers. FWMAVs could be used in many applications, such as exploring airspace with an animal-like stealth flying vehicle. It is a challenge to learn and invent a new type of flapping wing system [1]. Therefore, there are many types of FWMAVs nowadays, for example, beetle robots [2], [3], bee robots [4], [5], butterfly robots [6]–[8], dragonfly robots [9], and other animal-like flying robots [5], [10], [11]. Flapping wing robots can be divided into three groups according to the number of wings. They are robots with two wings [12], [13], robots with four wings or X-wings [14], and robots with eight or more wings [15].

The main investigation of these robots has focused on 4 parts: the power source, the actuator, the wing mechanism, and the wing [16], [17]. The first part is the power source which provides the input power to drive the actuator. The second part is the actuator that converts the electrical energy or elastic potential energy into mechanical energy [18], [19], such as an electric motor and an elastic rubber band [7], [20]. The third part is the flapping wing mechanism which converts the actuator motion into the desired wing motion. Finally, the fourth part is the wings. The wing parameters include the geometry, the structural material, and the number of wings. The flapping mechanism and wing parameters affect the aerodynamic jet flow and thrust generation. For example, a two-winged robot generates thrust through vortex capture and clap-and-fling motion [21], and a four-winged robot generates thrust through clap-and-peel motion [22].

In four-winged robots, the clap-and-peel motion occurs on the side of the body where the upper and lower wings are clapping [23]. Tay et al, [23] has studied the flapping pattern of four-winged robots and reported the CFD results of aerodynamic effects. It has higher aerodynamic efficiency than the two-winged robot because the two-winged flapping motion generates power only in the downstroke and uses the upstroke for recovery. Therefore, this study analyzes the aerodynamic parameters and power conversion characteristics of a four-winged robot under different flight conditions to provide guideline values for selecting actuators for other four-winged robots.

Many studies have investigated robots with four flapping wings in terms of aerodynamic parameters such as wing size and shape, flapping frequency, aerodynamic flow, thrust force, thrust coefficient, power consumption, and body velocity [24]–[28]. Most studies have reported either hover tests [29] or forward flight tests [30], [31]. However, none of the studies compared the aerodynamic parameters of the same flying robot in different flight modes, i.e., fixed-base flutter, hover and forward flight modes. Therefore, the objective of this study is to

Manuscript received August 3, 2022; revised November 10, 2022.
Corresponding author is P. Smithmaitrie

doi: 10.18178/ijmerr.11.12.891-900

understand the relationship between the power consumption and aerodynamic power generation of the four-winged robot in different flight modes. The aerodynamic parameters are flapping frequency, air jet velocity, thrust coefficient, thrust and power conversion characteristics. The three test modes are fixed-base flutter, hover, and vertical forward flight. The experimental results show the performance of the robot in converting input power to aerodynamic power in different flight modes. The findings obtained in this study provide an indication of the system-specific performance, power conversion, and actuator requirements to select an actuator and design a flapping mechanism and wings suitable for different flight modes.

II. The Power Flow of the Flapping Wing Robot System

The block diagram of the energy flow of a flapping wing robot system is shown in Fig. 1. A lithium polymer battery was chosen as the energy source for the flying robot because it has a high specific power-to-weight ratio. The supplied electrical energy flows through the electromechanical subsystem, which includes the motor, flapping mechanism and wings, to generate the thrust (aerodynamic force) that propels the robot body in the air.

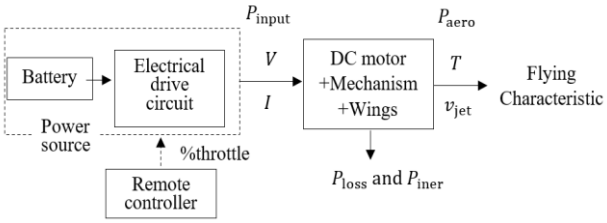

Figure 1. The system block diagram of the FWMAV.

The flapping wing robot is started by adjusting a throttle button on the remote control. The remote control transmits the RF control signal to the RF receiver on the electronic circuit board of the robot. The electronic circuit controls the supplied voltage, according to the received throttle control signal, in the form of pulse width modulation (PWM) to drive the motor. The effective driven voltage depends on the average value of the % duty cycle. The electrical input power (P_{input}) is calculated according to [32]

$$P_{input} = I_{avg} V_{avg} \quad (1)$$

where I_{avg} is the average current and V_{avg} is the average voltage across the motor. The supplied current I_{avg} is determined by measuring the average voltage across a small resistor, which is explained later in the experimental setup.

The motor converts electrical power into mechanical power in the form of rotational speed (ω) and torque (τ). The motor shaft drives gears and links that cause the leading edge of the wing to flap.

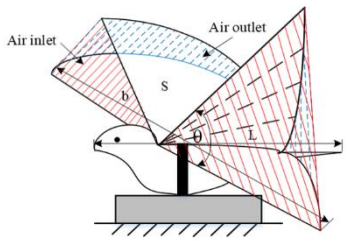

Figure 2. The geometry of the robot with four flapping wings.

When the wings beat at a flapping frequency (*f*), the air in front of the wing is sucked into the wing and expelled on the back side like a jet stream. The geometry of the robot, the air inlet and outlet are shown in Fig. 2. The flapping of the wings generates the propulsion. The flapping motion of the four wings that generates the main jet is called the clap-and-peel motion [33]. The reaction to the propulsion, called thrust (*T*), drives the robot body in the forward direction. The thrust can be described as follows

$$T = \rho \Delta v_{jet}^2 A_o C_T \quad (2)$$

where ρ is the air density, Δv_{jet} is the relative jet velocity, A_o is the area of the air outlet, C_T is the thrust coefficient which depends on the wing aspect ratio (AR) [1], air velocity and flapping frequency. The thrust coefficient can be experimentally determined.

In the case of a robot flying forward in a vertical direction, thrust is the force that moves the robot body. It can be derived by Newton's second law as

$$T = ma + mg + D \quad (3)$$

where *m* is the total mass of the system, *g* is gravity, *a* is the body acceleration which can be determined by using the image tracking method, and *D* is the drag force which can be expressed as follows

$$D = \rho \Delta v_{air\_impact}^2 A_i C_D \quad (4)$$

where Δv_{air_impact} is the relative impact velocity of the air. The robot velocity can also be observed by image tracking, A_i is the cross-sectional area of the object including the air inlet, and C_D is the drag coefficient. When the velocity of the robot body is zero, the system provides only the power of the jet, i.e., the aerodynamic power (P_{aero}). It can be written as [34]

$$P_{aero} = T v_{jet} \quad (5)$$

However, there are some power losses in the system such as the power loss at the motor due to friction, back EMF and Joule power in the motor winding, and the power loss at the mechanical components due to friction, heat, damping effect, and structural deformation, including the

inertial power (P_{iner}) that makes the wing move. The efficiency of the system is defined as

$$\eta = \frac{P_{output}}{P_{input}} \quad (6)$$

Flight efficiency and power conversion depend on flight modes. The experimental setup and flight test conditions for studying aerodynamic parameters and performances in different flight modes are explained below.

III. Experimental Setup and Test Conditions

The components of the robotic system are labeled in Fig. 3. The robot with four wings consists of an electrical subsystem and a mechanical subsystem.

The electrical subsystem includes a battery and electronic circuitry. The battery is a 1-cell lithium polymer with a capacity of 70 mAh, 0.3 Wh. The weight of the battery is 2.10 g. The battery can power the robot for 10-15 minutes. The electronic circuit has an integrated RF receiver and motor drive circuit. The drive is a DC brushed motor. The DC motor has an idle speed of 40,000 rpm at 3.7 V. It is the only actuator that causes all four wings to flap via the mechanical subsystem. The mechanical subsystem consists of the body structure, the mechanism, and the wings. The gears and linkages convert the rotation of the motor shaft into the flapping motion of the wings, which generates the aerodynamic force. The body geometry of the flapping wing robot has already been described in Fig. 2. The system specifications of the four-wing robot are listed in Table I.

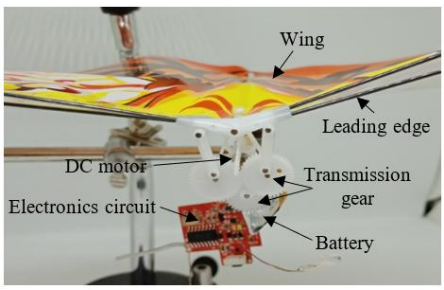

Figure 3. The components of the four-flapping-wing robot.

TABLE I. The Four-flapping-wing Robot Specification

Specification	
Wingspan (b)	27.5 cm
Wing area (S)	212.5 cm^2
Body length (L)	23.0 cm
Maximum flapping angle (θ)	80 deg.
Air outlet area behind the wing (A_o)	300 cm^2
Air inlet area (A_i)	264 cm^2
Weight	12.54 g
Battery	3.7 v
Charging time	15 – 20 min
Radio controlled frequency	2.4 GHz
RF communication range	30 – 50 m
Operation time	10 – 15 min

Three experiments are conducted to study the power flow and power conversion under different flight conditions. These are 1) the fixed base flapping test, in which the robot is attached with a force sensor to maintain its position on the ground and measure the generated force and the velocity of the air jet, 2) the hovering test, in which the robot hovers in the air, by adjusting the throttle to measure the velocity of the air jet and the percentage of throttle, and 3) the vertical flight test, in which the robot flies forward in the vertical direction along the guide wire. In this case, the thrust force lifts the robot into the air. Each test setup is explained in detail next.

A. The Fixed Base Flapping Test

The fixed base flapping test was developed to investigate the relationship between electrical input power and robot responses. The electrical input power driving the motor is measured using the circuit shown in Fig. 4. The motor is connected to the gearbox and flapping mechanism. A resistor of 1 Ω is inserted into the circuit to determine the current indirectly by measuring the voltage (V_R) across the resistor (R). When the throttle control signal is set to a certain value, the wing leading edges oscillate at a certain frequency corresponding to the motor speed. The voltage across the resistor V_R is very small compared to the voltage across the motor V. It is also assumed that the power loss in the resistor R is very small. Therefore, the driven voltage of the drive circuit is approximately equal to the voltage driving the motor. The current, I, is calculated by the voltage across the resistor,

$$I = \frac{V_R}{R} \quad (7)$$

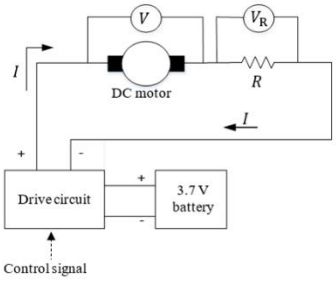

Figure 4. The measurement of the electric power.

The setup of the fixed base flapping test is shown in Fig. 5. The airflow through the fixed base flapping wing can be investigated using the smoke wire method, similar a previous report [21]. The thrust is measured with a force sensor under the fixed base. The flapping frequency is measured by image tracking with a high-speed video camera. The robot is mounted on the sensor bracket in a room without ventilation. The air velocity in front of the wing is about 0 m/s. The air velocity behind the wing is measured with an anemometer. The objective of this test is to investigate the relationship between jet velocity, thrust, % throttle and input power. Consequently, the average jet velocity and thrust are used in (2) to determine the thrust coefficient. In this experiment, the jet velocity resulting from all aerodynamic effects is measured.

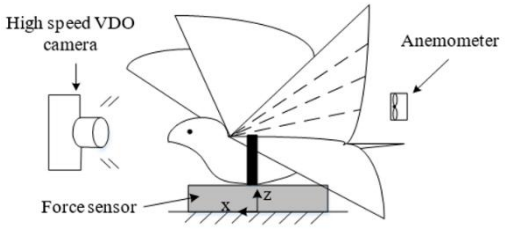

Figure 5. The thrust measurement of the fixed base flapping test.

The force sensor (ATI Industrial Automation, Gamma F/T sensor) is installed under the fixed base and records the generated thrust in the x-direction. The resolution of the force sensor is 0.0125 N in the x- and y- directions, and 0.025 N in the z-direction. The aerodynamic thrust is recorded at a sampling rate of 8 ms. The equipment and body weight in the vertical direction are excluded from the recorded data. The average value of thrust is recorded when the percent throttle control signal is increased from 0% to 100% throttle in 10% increments every 15 seconds. The flapping frequency is examined by tracking the flapping period of the wing motion. A digital camera (Sony Cyber-Shot DSC-RX100 V) is set to a high shutter speed to record the wing motion at 250 fps.

The jet velocity behind the wing is measured with a mini vane anemometer (DIGICON, DA-45) with a sampling rate of 16 ms. The jet velocity is recorded at different locations behind the wing (i.e., 0°, 22.5°, 45°, 67.5° and 90° relative to the body orientation) as shown in Fig. 6. The guidelines were drawn on the robot wing then the anemometer was held 1-cm away and perpendicular to the wing where the maximum air velocity is found. The air velocity is studied at different flapping frequencies according to the throttle control signal by recording the steady air velocity for five repetitions.

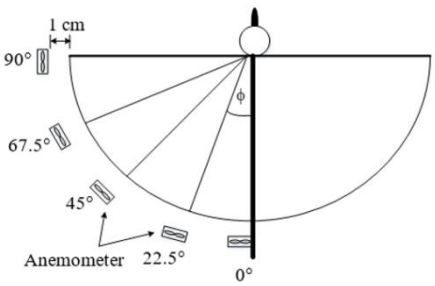

Figure 6. The measurement of the jet velocity behind the wing.

B. The Hovering Test

The goal of the hovering test is to determine the thrust and jet velocity that will allow the flapping robot to hover in the air. The test setup is shown in Fig. 7. During the test, the percentage of control throttle is increased until the robot begins to fly and can maintain its position in the air. Then, the jet velocity is measured in this hovering condition, similar to the fixed base flapping test.

Hovering is a form of free flight in which the measurement equipment cannot be attached to the robot. Consequently, the thrust cannot be measured directly. In this case, the thrust is calculated based on the relationship between power input and thrust coefficient from the fixed base flapping test. The generated hovering thrust is estimated by substituting the measured air velocity and the thrust coefficient in (2).

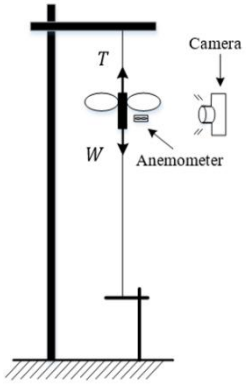

Figure 7. The measurement of jet velocity in the hovering test.

C. The Vertical Flight Test and Drag Measurement

The robot is constrained to move vertically to study the relationship between flight thrust and aerodynamic power. The vertical flight test is set up as shown in Fig. 8. The travel distance is one meter. The guide wire is made of nylon with a smooth surface and a diameter of 0.6 mm. A plastic tube is connected to the robot body to restrict the motion in the vertical direction along the guide wire. The contact friction between the nylon wire and the surface of the plastic tube is very low and negligible. The thrust is only generated by the flapping of the wings. The battery is installed inside the robot body. The flapping robot starts with an initial speed of zero at the lower end of the guide wire.

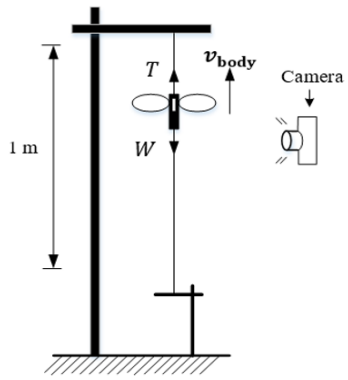

Figure 8. The vertical flight test setup.

In the thrust measurement, the robot is first started with different percentage throttle signals. The robot can take off with the minimum throttle of 70 %. Later, the percentage throttle is varied in 10 % increments until it reaches the maximum throttle of 100 %. The motion of the flying robot was recorded with the digital camera (Sony Cyber-Shot DSC-RX100V) at 50 frames per second (fps) and later interpreted as the velocity and acceleration of the body.

When the robot is moving in the air, there is an air resistance, called drag, which is related to the impact velocity of the air, as described in (4). The drag on the robot body must be determined to estimate the actual

power output and system efficiency. The experimental setup for measuring the air resistance is shown in Fig. 9. The robot was installed on the fixed base with the force sensor. A fan generated the wind speed blowing toward the robot. The wind speed was set according to the travel speed of the robot in the vertical flight test. The effective drag cross-sectional area includes the cross-sectional area of the robot body and the air inlet area, because the flapping of the wings also affects the drag.

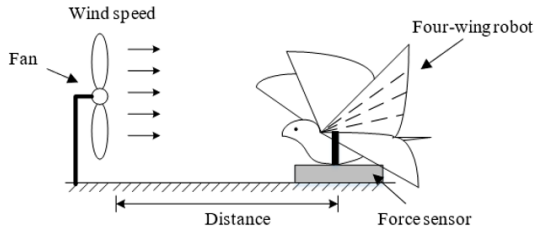

Figure 9. The setup of the drag experiment.

IV. Results

The three flapping tests were performed according to the experimental setups. The flight parameters and associated performance variables were determined as follows,

A. The Results of The Fixed Base Flapping Test

The electrical input power was measured during the fixed base flapping test. The percent duty cycle of the supplied voltage was measured when the percent throttle of the remote control was increased from 0-100 %, corresponding to a PWM duty cycle of 20.1-96.8 %. The corresponding average voltage was 1.18-3.79 V and the corresponding current was 0.20-0.66 A. Consequently, the electrical power driving the motor ranged from 0.24-2.50 W. The electrical input power that drove the system according to the percent throttle is shown in Table II.

TABLE II. The Input Power in the Fixed Base Flapping Test

% throttle	% duty cycle	V_{avg}	I_{avg}	P_{input}
0	0	0	0	0
10	20.1	1.18	0.20	0.24
20	24.2	1.85	0.21	0.39
30	31.9	2.11	0.24	0.51
40	36.5	2.51	0.31	0.78
50	42.3	2.55	0.34	0.87
60	54.3	2.69	0.39	1.05
70	59.6	3.07	0.49	1.50
80	72.3	3.26	0.51	1.66
90	83.7	3.57	0.52	1.86
100	96.8	3.79	0.66	2.50

The wing flapping period was recorded when the % throttle control signal changed by image tracking with an error of ±0.05 s. Consequently, the flapping frequency can be related to the power demand as shown in Fig. 10. It can be seen that the wing mechanism beats in a frequency range of 8.9-19.2 Hz and the robot requires more power as the flapping frequency increases.

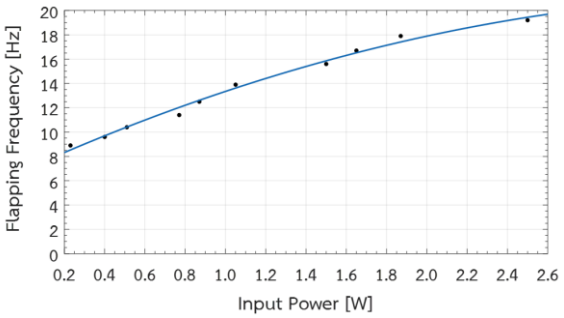

Figure 10. The relationship between input power and flapping frequency.

When the wings moved up and down rapidly, air was sucked in front of the wing and released at the back of the wing with increased air velocity, propelling the robot forward. The jet velocity was measured at different locations to record the velocity profile, as shown in Fig. 11. The air velocity component in the x-direction produced the forward thrust. The magnitude of the lateral air velocity components in the y-direction of the left and right wings were approximately the same, but in opposite directions. Therefore, the net lateral force was approximately zero.

The effect of the clap-peel-fling motion creates the air velocity profile on the back side of the wing. The lowest velocity occurred at the wing tip (90° relative to body orientation). The maximum velocity was found at the 22.5° position relative to the body orientation because this is where the largest moving wing area is. The local jet velocity at different input powers was measured as shown in Fig. 12. It clearly shows that the jet velocity profile maintains its shape, and the velocity increases with increasing input power. This phenomenon is consistent with other studies [35], [36].

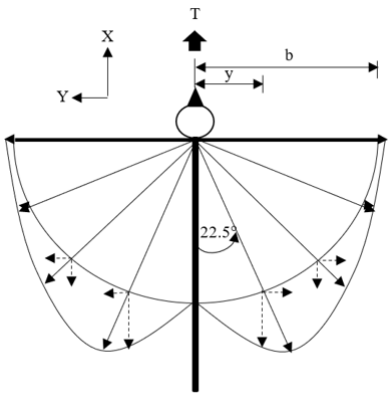

Figure 11. The air velocity profile of the robot with four flapping wings.

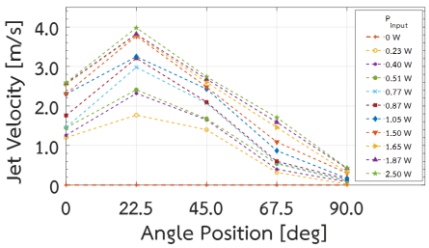

Figure 12. The relationship between the air velocity profile and input power.

The fixed base flapping test shows that the average jet velocity increased from 0.942-2.290 m/s when the percentage throttling was increased from 10-100 %. The relationship between the input power, average jet velocity and Reynolds number (Re) is shown in Fig. 13. The Reynolds number is a relative parameter representing the flow and viscosity effects of air [1].

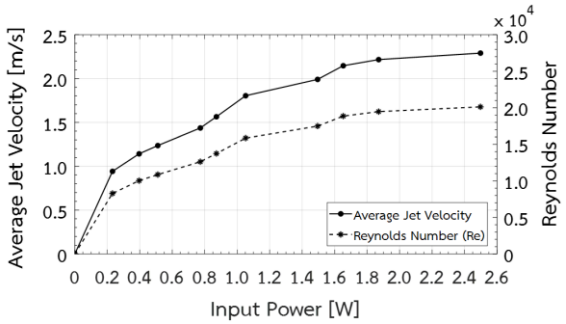

Figure 13. The relationship between the input power, average jet velocity and Reynolds number.

When the throttle was increased from 10-100%, the wings flapped and air was released at the back, resulting in the forward reaction thrust in the x-direction measured by the force sensor. The relationship between the flapping thrust and input power is shown in Fig. 14. The result shows that the average thrust increases with increasing input power. For a given input power, the thrust varies due to the flapping characteristics of the wing. For example, at a given input power of 1.05 W (60 % throttle), the robot produced forward thrust in the range of 0.06-0.115 N. The oscillating thrust occurred because the flapping wings created an unsteady air jet and vortex [21]. This aerodynamic thrust oscillation was caused by the air vortex at the leading and trailing edges [7].

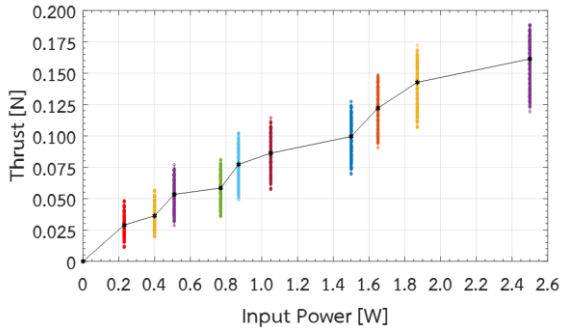

Figure 14. The relationship between the input power and flapping thrust.

To understand the thrust behavior, the thrust oscillation in flapping cycles was studied and analyzed as shown in Fig. 15. It can be seen that the thrust oscillation repeats every three flapping cycles. This confirms that the thrust does not have to repeat in every cycle, but it can repeat once every few flapping cycles due to the air vortex formation, as it was the case in the robot with two flapping wings [21]. It should be noted that the thrust variation depends on the flapping pattern and frequency.

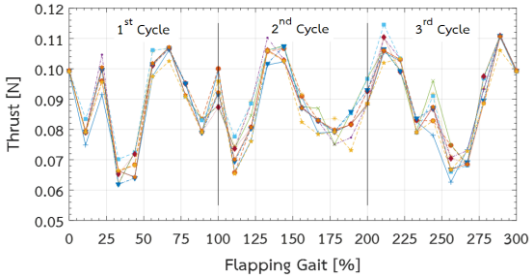

Figure 15. The generated thrust in the flapping gait at an input power of 1.05 W.

The thrust coefficient is calculated based on (2) by substituting the measured average jet velocity and thrust. The air density at room temperature (25 °C) is 1.18 kg/m^3 and A_o is 300 cm^2 in this case. The relationship between the average jet velocity and thrust coefficient is shown in Fig. 16.

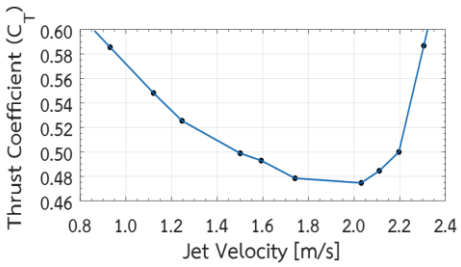

Figure 16. The relationship between the average jet velocity and thrust coefficient.

At low flapping frequency and low jet velocity, the generated thrust is not enough to lift the robot and fly. However, the thrust in the slow flapping condition is still useful for gliding flight when the robot is already in the air. The robot uses the low velocity of the air jet and the high thrust coefficient to generate additional thrust in combination with the lift force generated by body and wing shapes. The same gliding behavior with slow wing beats is naturally performed by flying animals. Fig. 17 shows the relationship between the average flapping thrust and thrust coefficient. When jet velocity cannot be directly observed in free flapping flight, the thrust and corresponding thrust coefficient can be used to estimate the jet velocity. The obtained thrust coefficient is the average thrust coefficient which indicates the performance of the wing system in converting jet velocity to thrust. However, thrust, jet velocity, and thrust coefficient vary within a wing stroke cycle (Fig.15).

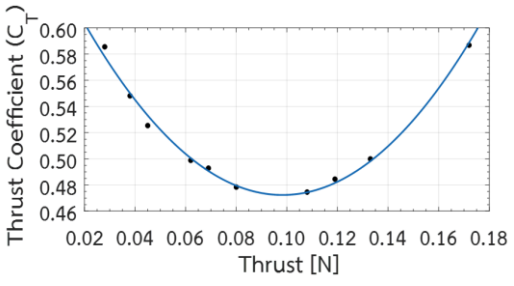

Figure 17. The relationship between the average thrust and thrust coefficient.

The relationship between the input power, aerodynamic power, and percent throttle is shown in Fig. 18. The electrical input power was in the range of 0.23-2.20 W. According to (5), the corresponding aerodynamic power was in a range of 0.027-0.369 W. The ratio between the aerodynamic output power and the electrical input power implies the conversion efficiency of the robot system during the flapping on the fixed base.

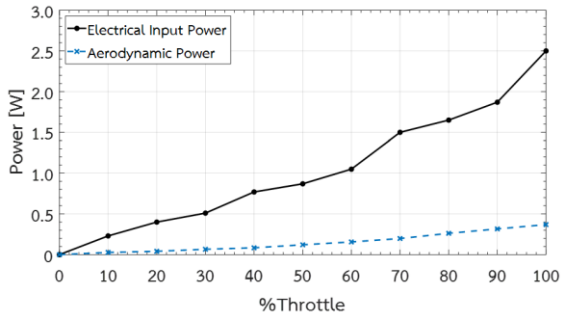

Figure 18. The relationship between the percent throttle, electrical input power, and aerodynamic power of the fixed base flapping test.

B. The Result of the Hovering Flight Test

The aerodynamic hovering performance and related parameters are summarized in Table III.

TABLE III. THE HOVERING FLIGHT PARAMETERS

Parameters	Value
Throttle	50-70 %
Input power (P_{input})	1.140 W
Local average jet speed	
0°	1.45 m/s
22.5°	3.75 m/s
45°	2.70 m/s
67.5°	1.86 m/s
90°	0.76 m/s
Avg	2.10 m/s
Average thrust (T)	0.118 N
Thrust coefficient (C_T)	0.485
Average aerodynamic power (P_{aero})	0.249 W

In order to hover the robot, the throttle must be regularly adjusted in a range of 50-70 %. The system requires an input power of 0.872-1.495 W or an average input power of 1.140 W. If the percentage throttle is less than 50% (0.872 W), the robot will not be able to take off and hover. While the robot is hovering, the height of the robot fluctuates in a range of 1-5 cm with a measured average jet velocity of 2.10 m/s. This average jet velocity is just sufficient to generate the hovering thrust. From the previous test in Fig. 16, the corresponding C_T is 0.485. According to (2), an average hovering thrust of 0.118 N is calculated, which is close to the body weight of 0.123 N. However, the hovering thrust constantly fluctuates due to the fluttering airflow.

C. The Results of the Vertical Flight Test

The robot flew in the vertical direction when the throttle was set to at least 70%. When the throttle was set to 70 %, the robot took off and flew slowly at 0.06 m/s. At full throttle, the robot took off quickly and flew at 1.45 m/s because the corresponding thrust of 0.163 N is greater than the body weight (0.123 N). Using the recorded VDO, the vertical velocity of the robot was determined and plotted against the travel distance, as shown in Fig. 19. The flight velocity depends on the input power that associated with the % throttle. The robot velocity increased from the initial start position until it reached the maximum velocity within 0.3 m. After that, the robot was able to maintain the velocity. The relationship between the vertical flight velocity and corresponding % throttle is shown in Fig. 19. However, there were some cases where the travel velocity suddenly changed because the robot body rotated during the flight. The robot rotation may occur due to the induced vortex force around the robot, for example, when the travel distance is 0.45 m and the throttle is 90 % in Fig. 19. However, when the throttle is 100 %, the body rotation does not occur because the induced vortex is far away from the robot. At 70 % and 80 % throttling, the induced vortex force is not strong enough to rotate the robot. The highest flight speed was achieved at 100 % throttling. The result shows that the robot consumes the electrical input power in a range of 1.5-2.5 W (70-100% throttling), resulting in an average vertical body velocity of 0.06-1.45 m/s.

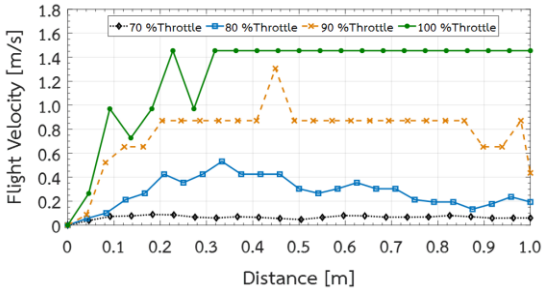

Figure 19. The relationship between the travel distance and vertical flight velocity.

The constant final flight velocity implies that the robot moves with zero acceleration. This means that air drag affects the robot dynamics by counteracting the thrust effort. For a given robot model, air drag can be experimentally determined, as mentioned earlier. The drag was measured with the force sensor when the robot faced the impact airflow with the same relative airspeed. The test setup is shown in Fig. 20. The magnitude of the drag is proportional to the square of the relative velocity of the impact air, as described in (4).

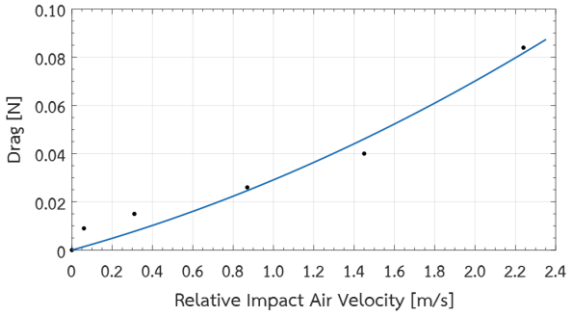

Figure 20. The relationship between the air impact velocity and drag.

Even though the net driving force approaches zero due to the counteracting effect of the drag causing the constant final velocity (Fig. 19), the thrust is still generated to propel the robot upward. The thrust can be determined by

(3) when the acceleration in the constant velocity condition is approximately zero. Therefore, the generated thrust corresponding to the input power can be determined as shown in Fig. 21.

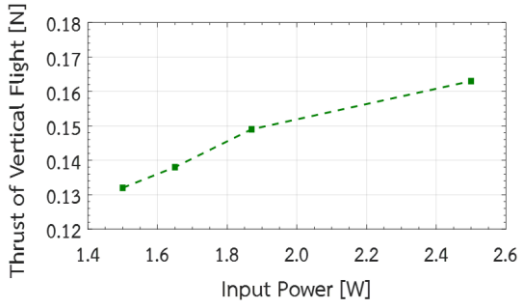

Figure 21. The relationship between the input power and thrust.

Based on the result of the fixed base test (Fig. 17), the thrust and corresponding thrust coefficient are used to calculate the jet velocity. Hence, the relationship between the jet velocity and input power can be estimated by (2), as shown in Fig. 22. It can be seen that the jet velocity and Reynolds number increase as the input power increases because an increase in flapping frequency produces a higher jet velocity.

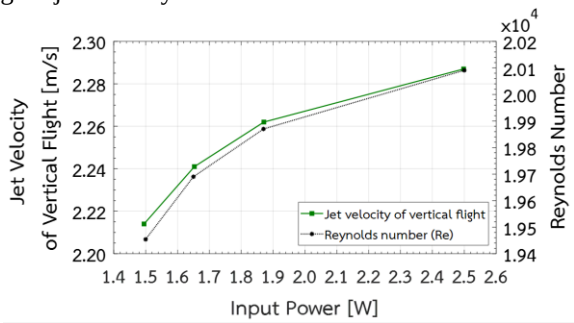

Figure 22. The relationship between the input power, jet velocity and Reynolds number.

D. The Flapping Flight Characteristics and Power Conversion

In this section, the aerodynamic parameters and input power of all flapping tests are compared. The comparison of the average jet velocity in different flight modes is shown Fig. 23. The average hovering jet velocity is maintained at 2.10 m/s, while the required power varies in a range of 0.9-1.6 W or the average power of 1.14 W. It is noted that the average hovering jet velocity is higher than that of the fixed base flapping jet velocity at the same input power. This is because, in the fixed base system, energy can be lost through the support. Thus, there is less energy left to generate the jet velocity. When the input power increases above 1.50 W, the flight behavior of the robot changes from hovering to flying in the vertical direction with a slightly higher jet velocity. In the vertical flight mode, the jet velocity slightly increases as the input power increases from 1.5-2.5 W. This implies that the aerodynamic power increases slightly with the jet velocity. That is, the increased portion of the input power is converted into the aerodynamic power that drives the robot body.

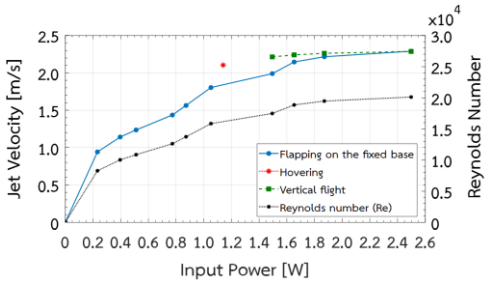

Figure 23. The comparison of average jet velocity in different flight modes.

The fixed base flapping test gives an ideal indication of how much aerodynamic power or thrust can generate with respect to the jet velocity. Fig. 24 compares the generated thrust in different flight modes. The fixed base flutter produced thrust less than the hover mode for the same input power, due to the loss of energy at the support, as mentioned earlier. In the vertical flight mode, the thrust is greater than the fixed base flapping thrust for the same reason.

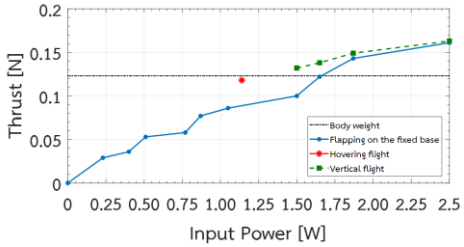

Figure 24. The comparison of thrust in different flight modes.

The electrical input power and aerodynamic power of all tests are compared as shown in Fig. 25. The power conversion efficiency can be determined by considering the ratio between the generated power and input power in each flight condition. The result shows that the efficiency of converting the electrical input power to the hovering aerodynamic power is 21.8 %. Although, the thrust was generated, the work done by the thrust is zero since no flight distance is covered. The generated hovering thrust was used to lift the robot's body weight and maintain its position in the air with little fluctuation due to flapping.

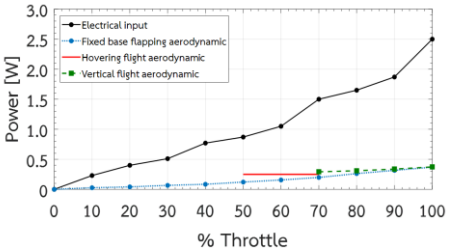

Figure 25. The comparison of the input and generated powers of all flapping tests.

In addition, the ability of the robot structure and flapping mechanism to convert aerodynamic power can be evaluated by the fixed base flapping test. That is, the input power is converted to the aerodynamic power without moving the body over the entire range of the throttle control signal, by accepting some energy loss at the support.

When the robot flies in the vertical direction, some power losses occur due to air resistance and low friction on the guide wire. All tested flight performance and aerodynamic parameters are summarized in Table IV. Compared to the hover condition, the vertically flying robot consumes higher input power to generate the higher thrust that propels it into the air. The consumed power increases as the speed of the robot increases. Therefore, the ratio of average jet velocity to weight is an important parameter for the development of a flying robot. The result shows that the four-wing mechanism can generate a jet velocity to weight ratio of more than 0.167 m/(s-g).

TABLE IV. FLIGHT PERFORMANCE AND AERODYNAMIC PARAMETERS OF THE FOUR-FLAPPING-WING ROBOT

Parameter	Hovering mode	Vertical flight mode
f	12.5-15.6 Hz	15.6 - 19.2 Hz
P_{input}/W	0.091 W/g	0.120-0.199 W/g
P_{output}/W	0.020 W/g	0.023-0.030 W/g
η	21.84%	19.49-14.91%
v_{jet}/W	0.167 m/(s-g)	0.177-0.182 m/(s-g)
C_T	0.485	0.488-0.565

The power-to-weight ratio of the robot is also a crucial parameter for assessing hovering and flight capabilities. In this case, the hover power per body weight is 0.020 W/g and the vertical flight power per body weight is 0.025 W/g. These specific power requirements are the same for all types of actuators. However, the efficiency of the system depends on the wing shape and flapping mechanism, which affect the generated aerodynamic power.

V. CONCLUSION

The experimental investigation of the robot with four flapping wings was conducted in three different flapping tests to study the aerodynamic parameters and power conversion characteristics. The three tests were fixed base flapping, hovering, and vertical flight. The results showed that the robotic system generated an average jet velocity of 0.94-2.29 m/s by consuming an input power of 0.23-2.50 W. The presented wing design produced the local maximum air velocity at 22.5 ° relative to the body orientation. Later, the hover test showed that the robot hovered at a throttle control signal of 50-70%, corresponding to an average input power of 1.14 W or an average specific power consumption of 0.091 W/g. Accordingly, the estimated hover thrust fluctuated around 0.118 N, which was just enough to lift the body weight of 0.123 N and maintain the altitude in the air, with the oscillation caused by the wing beat. The flapping frequency in hover was 12.5-15.6 Hz with an average jet velocity of 2.10 m/s. The robotic system had an efficiency of 21.84 % in converting the electrical input power to hovering aerodynamic power. In the vertical flight test, the robot required a higher power of 1.50-2.50 W or a specific power consumption of 0.120-0.199 W/g to fly upward. The flapping frequency in vertical flight was 15.6-19.2 Hz. The efficiency of input power conversion to aerodynamic power was 19.49-14.91 %. In this study, the aerodynamic parameters of the four-flapping wing, specific power consumption of the robot, efficiency of power conversion between electrical input power and aerodynamic power in different flight modes were experimentally investigated. These can be used as a guide for the design of a robot with four flapping wings and the selection of any type flapping actuator.

ACKNOWLEDGMENT

This research was supported in part by National Science, Research and Innovation Fund (NSRF) and Prince of Songkla University (Grant No. ENG6601312S). The authors gratefully acknowledge the graduate research scholarship from Faculty of Engineering, Prince of Songkla University. The authors gratefully acknowledge the support of the Smart Mechatronic Research Unit, Faculty of Engineering, Prince of Songkla University, which made the high performance measurement device possible.

CONFLICT OF INTEREST

All authors declare no conflicts of interest.

AUTHORS CONTRIBUTIONS

Kamonrat Tangudomkit conducted the research and drafted the manuscript; Pruittikorn Smithmaitrie is the principal investigator and corresponding author, analyzed the data, revised the manuscript. All authors had approved the final version.

REFERENCES

[1] W. Shyy, *An Introduction to Flapping Wing Aerodynamics*, 1 edition. Cambridge. New York: Cambridge University Press, 2013.

[2] P. R. Bhayu, Q. V. Nguyen, H. C. Park, N. S. Goo, and D. Byun, "Artificial cambered-wing for a beetle-mimicking flapper," *J Bionic Eng*, vol. 7, no. S4, pp. S130–S136, Dec. 2010.

[3] A. Muhammad, Q. V. Nguyen, H. C. Park, D. Y. Hwang, D. Byun, and N. S. Goo, "Improvement of artificial foldable wing models by mimicking the unfolding/folding mechanism of a beetle hind wing," *J Bionic Eng*, vol. 7, no. 2, pp. 134–141, Jun. 2010.

[4] B. M. Finio and R. J. Wood, "Distributed power and control actuation in the thoracic mechanics of a robotic insect," *Bioinspir. Biomim.*, vol. 5, no. 4, p. 045006, Dec. 2010.

[5] M. F. Bin Abas, A. S. Bin Mohd Rafie, H. Bin Yusoff, and K. A. Bin Ahmad, "Flapping wing micro-aerial-vehicle: Kinematics, membranes, and flapping mechanisms of ornithopter and insect flight," *Chinese Journal of Aeronautics*, vol. 29, no. 5, pp. 1159–1177, Oct. 2016.

[6] T. Fujikawa, K. Hirakawa, S. Okuma, T. Udagawa, S. Nakano, and K. Kikuchi, "Development of a small flapping robot," *Mechanical Systems and Signal Processing*, vol. 22, no. 6, pp. 1304–1315, Aug. 2008.

[7] H. Tanaka, K. Matsumoto, and I. Shimoyama, "Design and performance of micromolded plastic butterfly wings on butterfly ornithopter," in *Proc. 2008 IEEE/RSJ International Conference on Intelligent Robots and Systems*, Nice, Sep. 2008, pp. 3095–3100.

[8] B. H. Chen, L. S. Chen, Y. Lu, Z. J. Wang, and P. C. Lin, "Design of a butterfly ornithopter," *Journal of Applied Science and Engineering*, vol. 19, no. 1, Jan. 2016.

[9] T. Kizu, M. Inoue, K. Yoshino, and K. Hiraki, "Development of dragonfly-like flapping robot," in *Proc. 2016 4th Intl Conf on Applied Computing and Information Technology/3rd Intl Conf on Computational Science/Intelligence and Applied Informatics/1st Intl Conf on Big Data, Cloud Computing, Data Science &*

Engineering (ACIT-CSII-BCD), Las Vegas, NV, USA, Dec. 2016, pp. 87–92.
[10] M. H. Rosen, G. le Pivain, R. Sahai, N. T. Jafferis, and R. J. Wood, "Development of a 3.2g untethered flapping-wing platform for flight energetics and control experiments," in *Proc. 2016 IEEE International Conference on Robotics and Automation (ICRA)*, Stockholm, Sweden, May 2016, pp. 3227–3233.
[11] G. K. Lau, Y. W. Chin, J. T. W. Goh, and R. J. Wood, "Dipteran-insect-inspired thoracic mechanism with nonlinear stiffness to save inertial power of flapping-wing flight," *IEEE Trans. Robot.*, vol. 30, no. 5, pp. 1187–1197, Oct. 2014.
[12] A. Jennings, M. Mayhew, and J. Black, "Video measurements of instantaneous forces of flapping wing vehicles," *Mechanical Systems and Signal Processing*, vol. 64–65, pp. 325–336, Dec. 2015.
[13] N. Gans, A. Chakravarthy, and R. Albertani, "Analysis of kinematics and dynamics of Butterflies in natural flight, with estimation of occluded data," p. 4.
[14] G. C. H. E. de Croon, K. M. E. de Clercq, R. Ruijsink, B. Remes, and C. de Wagter, "Design, aerodynamics, and vision-based control of the DelFly," *International Journal of Micro Air Vehicles*, vol. 1, no. 2, pp. 71–97, Jun. 2009.
[15] H. K. Jung, J. S. Choi, C. Wang, and G. J. Park, "Analysis and fabrication of unconventional flapping wing air vehicles," *International Journal of Micro Air Vehicles*, vol. 7, no. 1, pp. 71–88, Mar. 2015.
[16] K. Mazaheri and A. Ebrahimi, "Experimental investigation of the effect of chordwise flexibility on the aerodynamics of flapping wings in hovering flight," *Journal of Fluids and Structures*, vol. 26, no. 4, pp. 544–558, May 2010.
[17] M. Karpelson, J. P. Whitney, Gu-Yeon Wei, and R. J. Wood, "Energetics of flapping-wing robotic insects: towards autonomous hovering flight," in *Proc. 2010 IEEE/RSJ International Conference on Intelligent Robots and Systems*, Taipei, Oct. 2010, pp. 1630–1637.
[18] Q. V. Nguyen, Q. T. Truong, H. C. Park, N. S. Goo, and D. Byun, "Measurement of force produced by an insect-mimicking flapping-wing system," *J Bionic Eng*, vol. 7, no. S4, pp. S94–S102, Dec. 2010.
[19] M. Hassanalian, A. Abdelkefi, M. Wei, and S. Ziaei-Rad, "A novel methodology for wing sizing of bio-inspired flapping wing micro air vehicles: Theory and prototype," *Acta Mech*, vol. 228, no. 3, pp. 1097–1113, Mar. 2017.
[20] H. Tanaka and I. Shimoyama, "Forward flight of swallowtail butterfly with simple flapping motion," *Bioinspir. Biomim.*, vol. 5, no. 2, p. 026003, Jun. 2010.
[21] K. Tangudomkit and P. Smithmaitrie, "Aerodynamic experimental investigation and analysis of the flow and thrust generation of the flexible flat flapping wing robot," in *Proc. 2021 Second International Symposium on Instrumentation, Control, Artificial Intelligence, and Robotics (ICA-SYMP)*, Bangkok, Thailand, Jan. 2021, pp. 1–6.
[22] M. Percin, B. van Oudheusden, and B. Remes, "Flow structures around a flapping-wing micro air vehicle performing a clap-and-peel motion," *AIAA Journal*, vol. 55, no. 4, pp. 1251–1264, Apr. 2017.
[23] W. B. Tay, B. W. van Oudheusden, and H. Bijl, "Numerical simulation of a flapping four-wing micro-aerial vehicle," *Journal of Fluids and Structures*, vol. 55, pp. 237–261, May 2015.
[24] M. Groen, B. Bruggeman, B. Remes, R. Ruijsink, B. van Oudheusden, and H. Bijl, "Improving flight performance of the flapping wing MAV DelFly II," p. 17.
[25] P. Zdunich *et al.*, "Development and testing of the mentor flapping-wing micro air vehicle," *Journal of Aircraft*, vol. 44, no. 5, pp. 1701–1711, Sep. 2007.
[26] S. Deng, "Experimental investigation of the flapping performance on 'Delfly Micro,'" p. 8, 2013.
[27] S. Deng, M. Percin, B. van Oudheusden, B. Remes, and A. Tenaglia, "Force and flowfield measurements of a bio-inspired flapping MAV 'Delfly Micro,'" presented at the 32nd AIAA Applied Aerodynamics Conference, Atlanta, GA, Jun. 2014.
[28] M. Percin, B. W. van Oudheusden, G. C. H. E. de Croon, and B. Remes, "Force generation and wing deformation characteristics of a flapping-wing micro air vehicle 'DelFly II' in hovering flight," *Bioinspir. Biomim.*, vol. 11, no. 3, p. 036014, May 2016.
[29] K. De Clercq, R. de Kat, B. Remes, B. van Oudheusden, and H. Bijl, "Flow visualization and force measurements on a hovering flapping-wing MAV 'DelFly II,'" presented at the 39th AIAA Fluid Dynamics Conference, San Antonio, Texas, Jun. 2009.
[30] M. Percin, J. Eisma, B. Van Oudheusden, B. Remes, R. Ruijsink, and C. De Wagter, "Flow visualization in the wake of the flapping-wing MAV 'DelFly II' in forward flight," presented at the 30th AIAA Applied Aerodynamics Conference, New Orleans, Louisiana, Jun. 2012.
[31] M. Percin, B. W. van Oudheusden, H. E. Eisma, and B. D. W. Remes, "Three-dimensional vortex wake structure of a flapping-wing micro aerial vehicle in forward flight configuration," *Exp Fluids*, vol. 55, no. 9, p. 1806, Sep. 2014.
[32] A. Bontemps, S. Grondel, T. Vanneste, S. Dupont, and E. Cattan, "Modeling and evaluation of power transmission of flapping wing nano air vehicle," in *Proc. 2014 IEEE/ASME 10th International Conference on Mechatronic and Embedded Systems and Applications (MESA)*, Senigallia, Italy, Sep. 2014, pp. 1–6.
[33] M. Karpelson, Gu-Yeon Wei, and R. J. Wood, "A review of actuation and power electronics options for flapping-wing robotic insects," in *Proc. 2008 IEEE International Conference on Robotics and Automation*, Pasadena, CA, USA, May 2008, pp. 779–786.
[34] N. Cumpsty, *Jet Propulsion: A Simple Guide to the Aerodynamic and Thermodynamic Design and Performance of Jet Engines*, 2nd ed. Cambridge University Press, 2003.
[35] L. J. Yang *et al.*, "The wind tunnel test and unsteady CFD of an ornithopter formation," in *Innovative Design and Development Practices in Aerospace and Automotive Engineering*, R. P. Bajpai and U. Chandrasekhar, Eds. Singapore: Springer Singapore, 2017, pp. 9–16.
[36] L. J. Yang, A. L. Feng, H. C. Lee, B. Esakki, and W. He, "The three-dimensional flow simulation of a flapping wing," *Journal of Marine Science and Technology*, vol. 26, no. 3, pp. 297–308, 2018.

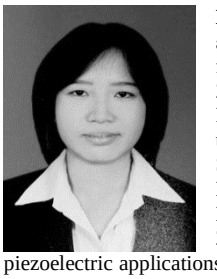

Kamonrat Tangudomkit earned the bachelor's and master's degrees in mechanical engineering from Prince of Songkla University, Thailand in 2008 and 2013, respectively. She is currently a Ph.D. student in the same program and university as the bachelor and master graduates. She has been a research assistant in Smart Mechatronics Research Team, Faculty of Engineering, Prince of Songkla University since 2009. Her research interests include piezoelectric applications, flapping wing aerodynamics and bio-inspired robots.

Pruittikorn Smithmaitrie earned a B.Eng. degree in mechanical engineering from Prince of Songkla University, Thailand, in 1996. After graduation, he received a scholarship from the Royal Thai Government to pursue his master's and doctoral degrees in the United States. In 2000, he earned a M.S. degree in mechanical engineering from Vanderbilt University, Nashville, TN. In 2004, he received his Ph.D. in mechanical engineering from the University of Kentucky, Lexington, KY.
Since 1996, he has been a member of the mechanical engineering faculty at Prince of Songkla University in 1996 and was appointed associate professor in 2008. His research interests include the analysis and design of mechatronic systems and piezoelectric applications.